Exploration of Excited State Deactivation Pathways of Adenine Monohydrates

Sermsiri Chaiwongwattana,[†,¶] Marin Sapunar,[†,¶] Aurora Ponzi,[†] Piero Decleva,[‡] and Nađa Došlić[*,†]

Ruđer Bošković Institute, Bijenička 54, 10000 Zagreb, Croatia, and Dipartimento di Scienze Chimiche, Università di Trieste, 34127 Trieste, Italy

E-mail: nadja.doslic@irb.hr

[*]To whom correspondence should be addressed
[†]Ruđer Bošković Institute
[‡]Università di Trieste
[¶]These authors contributed equally

Abstract

Binding of a single water molecule has a dramatic effect on the excited state lifetime of adenine. Here we report a joint nonadiabatic dynamics and reaction paths study aimed at understanding the sub-100 fs lifetime of adenine in the monohydrates. Our nonadiabatic dynamics simulations, performed using the ADC(2) electronic structure method, show a shortening of the excited state lifetime in the monohydrates with respect to bare adenine. However, the computed lifetimes were found to be significantly longer that the observed one.

By comparing the reaction pathways of several excited-state deactivation processes in adenine and adenine monohydrates, we show that electron-driven proton transfer from water to nitrogen atom $N3$ of the adenine ring may be the process responsible for the observed ultrafast decay. The inaccessibility of the electron-driven proton transfer pathway to trajectory-based nonadiabatic dynamics simulation is discussed.

1 Introduction

Understanding the photophysical mechanisms that prevent light induced damage in biomolecules is a fundamental scientific problem with a broad spectrum of potential applications.[1,2] In this context the photostability of nucleobases, and in particular of adenine, has been intensively investigated, both from the experimental,[3–9] and the theoretical side.[10–20] It is known that upon excitation at the origin of the first electronic band at 277 nm adenine deactivates to the ground electronic state following a biexponential kinetics with time constants of $\tau_1 \sim 100$ fs and $\tau_2 \sim 2$ ps.[8] However, a 700 cm^{-1} increase in the excitation energy leads to the reduction of the latter constant, which is the actual lifetime of the excited state, to only ~ 1 ps.[8] This suggests the existence of an energy barrier on the way to the conical intersection (CI) with the ground electronic state.

The pathways of adenine's decay after optical excitation to the bright $\pi\pi^*(L_a)$ state have been for a long time a matter of debate as different computational methods provide rather contrasting results.[11,13,17,18,20] In an early work Sobolewski and Domcke proposed that 9H-adenine (hereafter - adenine) decays following the $\pi\sigma^*$ pathway along the NH bond stretching coordinate of the azine group.[11] Although more recent computations find the $\pi\pi^*/\pi\sigma^*$ CI to be too high in energy to govern the deactivation, time resolved photoelectron spectroscopy experiments provide evidence that $\pi\sigma^*$ states may be involved in adenine relaxation.[6] A different mechanism was put forward on the basis of complete-active-space second-order perturbation theory (CASPT2) calculations indicating that the initially excited $\pi\pi^*(L_a)$ state crosses directly with the ground state following a barrierless reaction path.[13,17] More recently, nonadiabatic (NA) dynamics simulations performed using the algebraic diagrammatic construction to the second order [ADC(2)] method[21,22] pointed to internal conversion from the $\pi\pi^*$ to the $n\pi^*$ state with concomitant deformation of the six-membered ring at the $C2$ position leading to a minimum on the S_1 surface of mixed $n\pi^*$ and $\pi\pi^*$ character. The CI with the ground electronic state, S_0, is then reached by surmounting an energy barrier either along the $C2$ or $C6$ ring-puckering pathways.[20]

In water, following excitation at 263 nm, adenine decays biexponentially with time constants of $\tau_1 \sim 180$ fs and $\tau_2 \sim 8.8$ ps.[23] Here again, a number of theoretical studies addressed the mechanisms and time scales of adenine deactivation.[24–28] Serrano-Andrés and coworkers computed relaxation pathways of adenine in large water clusters using a combined Monte Carlo/CASPT2 approach.[25] Relevant adenine geometries were selected along both the $n\pi^*$ and $\pi\pi^*$ deactivation pathways. The authors have shown that the $\pi\pi^*$ state controls the decay and that the $n\pi^*$ state undergoes a strong destabilization in the water environment such that the $n\pi^*$ pathway becomes inaccessible from the initially populated $\pi\pi^*$ state. In the very recent ADC(2)-based NA dynamics study of 9H-adenine hexahydrates and 7H-adenine pentahydrates the electronic structure of water molecules has been explicitly taken into account.[28] It was found that the decrease of 9H-adenine excited state lifetime in water was due to a facilitated interconversion *via* ring puckering at position $C2$ following which can be considered to be the decay pathway of bare adenine - $\pi\pi^* \rightarrow n\pi^* \rightarrow S_0$.[28] However, the most important result of that study was that the ultrafast relaxation of 7H-adenine pentahydrates had purely electronic origins and was caused by electron transfer from water to 7H-adenine.

In circumstances in which the role of $\pi\pi^*$, $n\pi^*$ and $\pi\sigma^*$ states in the deactivation of solvated adenine is not completely understood, it may be of interest to consider the relaxation dynamics of the apparently simplest adenine-water cluster. However, a marked difference exists between adenine and its monohydrates as the attachment of a single water molecule to adenine decreases its lifetime by an order of magnitude.[29,30] Kang *et al.* reported time constants of 200 fs for excited state relaxation of adenine mono and dihydrates.[29] The remarkable lifetime decrease was attributed to the dissociation of the adenine-water hydrogen bond in the excited electronic state. Ritze *et al.* reported even shorter excited state lifetimes for $A(H_2O)$ and $A(H_2O)_3$ of the order of ~ 100 fs. In contrast to Kang *et al.* the authors here explained the ultrafast decay of adenine monohydrates in terms of stabilization of dissociative $\pi\sigma^*$ states.[30]

Even though a decade has passed from the publication of the experimental results, com-

putational studies of the excited state dynamics of adenine monohydrates seem to be unavailable in the literature. This work, aimed at disclosing the mechanism of ultrafast deactivation of adenine monohydrates, fills the gap. To this end we performed trajectory-based NA dynamics simulations of two conformers of adenine monohydrate whose presence in the jet has been recently established by vibrational spectroscopy.[31] Guided by the results of NA dynamics we located minima, transition states and relevant conical intersections along several deactivation pathways of adenine monohydrates. Throughout the work a systematic comparison with the relaxation paths of adenine is made. On this ground we propose a new and plausible mechanism for the deactivation of adenine monohydrates that is capable of explaining the striking experimental observations.

2 Computational Methods

The ground state geometries of several hydrogen bonded adenine monohydrates have been optimized using the MP2 method. The two lowest energy structures have been selected for subsequent investigations. Excited state computations were performed using the ADC(2) method[21,22] with the resolution of identity approximation (RI).[32,33] The standard Dunning correlation-consistent basis set augmented with polarization and diffuse functions (aug-cc-pVDZ) for N, C, O and H atoms has been used.[34]

ADC(2)-based NA dynamics trajectory simulations have been performed using an in-house software based on Tully's fewest switching surface hopping algorithm[35–38] and interfaced to Turbomole 6.4.[39] Elements of the NA couplings matrix were computed by constructing a formal CIS wave function using ADC(2) singles amplitudes followed by the evaluation of overlaps between singly excited SD at two time steps of the dynamics.[20,28,38] Standard parameters for NA dynamics simulations have been used.[38,40] Newton's equations were integrated in time steps of $\tau_1 = 0.5$ fs with the velocity-Verlet algorithm. Between nuclear time steps, the time-dependent Schrödinger equation was integrated using the Shampine and

Gordons predictor-corrector differential equation solver in time steps of $\tau_2 = 5 \times 10^{-5}$ fs.[41] The decoherence procedure of Granucci and Persico with $\alpha = 0.1\ E_h$ was employed.[42] The initial conditions were generated independently along each of the normal modes by using the ground state Wigner distribution for the harmonic oscillator thermal density at 100 K.[43] The required Hessian matrix was computed at the MP2/aug-cc-pVTZ level. To be used in molecular dynamics simulations, normal modes coordinates and velocities were transformed back to Cartesian.[44,45] Thus, our simulations account for zero point energy effects, but dynamical quantum effects, such as dynamical tunneling, cannot be described.

In total 50 ADC(2)/cc-pVDZ trajectories have been propagated in the manifold of the ground and threeexcited electronic states, starting from the bright $L_a(\pi\pi^*)$ state. To estimate the multireference character of the ground state, D_1 diagnostics were calculated along the trajectories.[39,46]

Subsequently, the photodeactivation pathways indicated by NA dynamics were systematically analyzed using the ADC(2)/aug-cc-pVDZ method. CI geometries were optimized using the sequential penalty constrained optimization method of Levine *et al.*[47] The default initial values of $\alpha = 0.025$ Hartree and $\sigma = 3.5$ were used. CI geometries were converged to the default energy gap of 0.001 Hartree (0.03 eV). Linearly interpolated reaction paths in internal coordinates (LIIC) were constructed in two regions: from adenine and adenine monohydrates Franck-Condon (FC) geometries to the minima, and from the minima to the respective CIs. Although LIIC barriers are upper limits to the true barriers, their computation permits a consistent comparison of the reaction pathways among the systems under consideration. Structures near the top of the LIIC barriers have been used as starting points for transition state optimization using the Trust Radius Image Minimization[48] algorithm. Cartesian geometries of the structures listed in Table 2 (*vide infra*) are given in Tables S1-S7. To check the effect of basis set superposition error on the results, the optimization of minima and transition states for all three systems have been performed using the larger def2-QZVPP basis set.[49]

The accuracy of the ADC(2) potential energy surfaces has been assessed against reference computations. Specifically, the first excited state of adenine and the most stable monohydrate at different key geometries was calculated using the CASPT2 method with the Molpro package.[50] The CASSCF reference orbitals were obtained in the state-averaged mode (SA-MCSCF), with two different active spaces: the first one consisted of 14 electrons in 10 orbitals (7 occupied orbitals and 3 virtual orbitals), the second one consisted of 14 electrons in 11 orbitals (7 occupied orbitals and 4 virtual orbitals). All valence π orbitals were included. The 1s core molecular orbitals were frozen in both cases. In the CASPT2 calculations, each state was treated separately and a level shift of 0.25 Eh was applied to the residuals.

3 Results and Discussion

3.1 Electronic structure calculations

Figure 1 (upper panel) shows the ground state minimum of the two lowest energy structures of adenine monohydrates as optimized at the MP2/aug-cc-pVDZ level of theory. In agreement with earlier studies in the most stable monohydrate, $A(H_2O)^{N3}$, the nitrogen atom $N3$ acts as a H-bond acceptor.[51] The structure in which the water molecule is hydrogen bonded to the amino group and the nitrogen atom $N7$, denoted $A(H_2O)^{N7}$, is found 0.93 kcal mol^{-1} higher in energy giving rise to a Boltzmann population of $\sim 15\%$. Both structures have been observed by Nosenko *et al.*[31]

Table 1 compiles the vertical excitation energies for the ground state equilibrium geometries of adenine, $A(H_2O)^{N3}$ and $A(H_2O)^{N7}$. In adenine the lowest excitation at 4.98 eV corresponds to an $n\pi^*$ transition. The two $\pi\pi^*$ transitions, found 5.09 (L_a) and 5.11 eV (L_b) above the ground state, are in good agreement with the experimental (vapor phase) band maximum at 244 nm (5.08 eV).[52] As expected, the binding of a single water molecule leads to destabilization of the $n\pi^*$ state and stabilization of the $\pi\pi^*(L_a)$ state by 0.05 and 0.19

eV in $A(H_2O)^{N3}$ and $A(H_2O)^{N7}$, respectively.

In all systems, geometry optimization of the absorbing $\pi\pi^*(L_a)$ state leads to minima with adiabatic excitation energies of 4.30, 4.38 and 4.25 eV in adenine, $A(H_2O)^{N3}$ and $A(H_2O)^{N7}$, respectively. In all three cases S_1 minima have mixed $n\pi^*$ and $\pi\pi^*$ character. Compared to the S_1 minimum of adenine, characterized by $C2$ pyramidalization angles of $\delta(C6N1C2H) = 169.8°$ and $\delta(C6N1C2N3) = 33.1°$, binding of water leads to structures with enhanced $C2$ pyramidalization (see Figure 1, lower panel). In $A(H_2O)^{N3}$ the six-membered ring is deformed by $\delta(C6N1C2H) = 172.9°$ and $\delta(C6N1C2N3) = 39.0°$ and in $A(H_2O)^{N7}$ by $\delta(C6N1C2H) = 174.7.8°$ and $\delta(C6N1C2N3) = 40.7°$. In going from adenine, to $A(H_2O)^{N3}$ and $A(H_2O)^{N7}$ the pyramidalization of the amino group decreases from $\delta(C5C6N7H) = 15.2°$ and $\delta(N1C6N7H) = -21.0°$ in adenine, to $\delta(C5C6N7H) = 12.2°$ and $\delta(N1C6N7H) = -19.0°$ in $A(H_2O)^{N3}$, and to $\delta(C5C6N7H) = 1.2°$ and $\delta(N1C6N7H) = -7.3°$ in $A(H_2O)^{N7}$. As mentioned, all minima have mixed $n\pi^*$ and $\pi\pi^*$ character, but a larger $\pi\pi^*$ contribution is found in $A(H_2O)^{N7}$ due to the near planar NH_2 group.

3.2 Nonadiabatic dynamics simulations

NA dynamics simulations initiated from the $L_a(\pi\pi^*)$ state revealed that within 1.5 ps of simulation time 24/36 $A(H_2O)^{N3}$ trajectories returned to the ground electronic state. In case of the less abundant conformer, $A(H_2O)^{N7}$, all 26 simulated trajectories deactivated to the ground state within 1.5 ps.

In terms of deactivation mechanisms, C_2 and C_6 ring-puckering channels known to govern the deactivation of adenine, are found to be the dominant deactivation channels of the monohydrates. Specifically, 42% of deactivations in $A(H_2O)^{N3}$ and 54% in $A(H_2O)^{N7}$ occurred *via* $C2$-puckered CI. The remaining trajectories ended mostly in $C6$-puckered CI or deactivated *via* what can be broadly described as water mediated relaxation (see Table 3 and Sec. 3.4).

Although our results are not fully comparable to those of Barbatti and coworkers owing

to differences in the basis set (cc-pVDZ *vs* aug-cc-pVDZ) and the number of electronic states involved in the computations (3 in the monohydrates, 2 in the hexahydrates), the computed fraction of trajectories ending in the $C2$-puckered CI finds good agreement with previous results indicating that 52% of adenine and 90% of hexahydrates trajectories ended up in the $C2$-puckered CI.[20,28] With respect to lifetimes, we found that in case of $A(H_2O)^{N3}$ the average lifetime along the $C2$-puckered pathways was 944 fs, while a slightly longer lifetime of 1190 fs was found for the $C6$ pathway. For $A(H_2O)^{N7}$ the lifetimes were shorter, 567 and 710 fs, for the $C2$ and $C6$ pathways, respectively. To check whether the addition of diffuse functions may alter these values and lead to ultrafast deactivation of the monohydrates, we launched a limited set of ADC(2)/aug-cc-pVDZ trajectories (10) for the more populated conformer $A(H_2O)^{N3}$. Within 500 fs of simulation time none of the trajectories crossed to the ground state. From these pieces of information two conclusions can be drawn. First, nonadiabatic dynamics simulations provide no evidence for the sub-100 fs lifetime of adenine monohydrates. Second, site specific solvation of the NH_2 group facilitates the deactivation of adenine monohydrates along both the $C2$ and $C6$ pathways. The latter result is consistent with the recent findings of Crespo-Hernández *et al.* indicating that the functional group at the $C6$ position plays an important role in modifying the rate of nonradiative relaxation to the ground state in various purine derivatives.[53]

3.3 Analysis of ring-puckering deactivation pathways

To understand the origin of the difference between the observed and computed lifetimes we first performed a comparative analysis of the $C2$ and $C6$ deactivation pathways among the three species, and subsequently focus on alternative deactivation mechanisms. Endpoints of NA dynamics trajectories, i.e., geometries on the S_1/S_0 CI seam, have been used as starting geometries for the optimization of CIs. Relative energies of optimized $C2$- and $C6$-puckered CI with respect to the geometry of vertical excitation (E_{FC}^{CI}) and of the S_1 minimum ($E_{S_1min}^{CI}$) are given in Table 2. For all three systems both the $C2$- and $C6$-puckered CIs are

found $0.9 - 1.1$ eV lower in energy than the FC geometry. With respect to S_1 minimum the CI geometries are $0.12 - 0.37$ eV lower in energy. To evaluate the barriers separating the minimum energy and CI geometries (see Table 2), LIIC potential energy profiles were computed. The information is displayed graphically on Figure 2 where the potential energies of the S_0 and S_1 states of adenine (top), $A(H_2O)^{N3}$ (middle) and $A(H_2O)^{N7}$ (bottom) along the $C2$ and $C6$ deactivation pathways are shown. Vertical lines separates two LIIC regions - the first going from the geometry of vertical excitation to the S_1 minimum, and the second from the minimum to the $C2$ (solid) and $C6$ (dashed) CIs. Note that in the monohydrates the CI between the bright state, $\pi\pi^*(L_a)$, and the $n\pi^*$ state is found in the vicinity of the FC geometry. It is evident that adenine, $A(H_2O)^{N3}$ and $A(H_2O)^{N7}$ share very similar reaction profiles in agreement with the computed moderate decrease of the excited state lifetime of the monohydrates.

A detailed comparison of the LIIC energy profiles reveals meaningful differences. With respect to the minimum energy structure the barriers on the $C2$ LIIC decrease from 0.43 to 0.33 and to 0.38 eV in going from adenine to $A(H_2O)^{N3}$ and to $A(H_2O)^{N7}$. On the contrary, the barriers on the $C6$ pathway increase from 0.66 to 0.76 and to 0.85 eV, in the same order. Thus, on the basis of energy considerations one would expect that, contrary to NA dynamics results, $A(H_2O)^{N3}$ deactivates faster than $A(H_2O)^{N7}$. Let us recollect, however, that the lifetime of the S_1 state depends on the barrier to be surmounted on the way to the CI, and on the accessibility of the S_1/S_0 CI seam. From the mass weighted root-mean square distances (RMSD) from the reference FC geometry, given in Figure 2, it is apparent that the S_1/S_0 CI seam is geometrically closer for $A(H_2O)^{N7}$ than for either $A(H_2O)^{N3}$ or bare adenine. The result is in accord with the computed faster relaxation of the former.

With respect to the suppression of the $C6$ pathway one sees that apart from being higher, the barriers on the $C6$ pathway are less accessible, than the ones on the $C2$ pathway. The reasons can be understood by analyzing the charge redistribution. The insets in Figure 2 display the difference in the electron densities between S_1 and S_0 electronic states for the FC

geometry, S_1 minimum and at the two CI geometries. The red (blue) areas indicate depletion (increase) of electron density in S_1 with respect to S_0. It is evident that the translocation of electron density from the carbon atom $C2$ to nitrogen atoms $N1$ and $N3$ drives the systems from the FC region to the corresponding $S_1(n\pi^*)$ minima. Once at the respective minima, the deactivation *via* $C2$ ring puckering requires a minor translocation of charge. On the contrary, to reach the $C6$-ring puckered CI a substantial flow of charge to the amino group is needed. This in turn leads to a major structural deformation resulting in a less favorable deactivation pathway.

The transition state (TS) geometries along the $C2$ and $C6$ deactivation pathways have been computed starting from the geometries at the top of LIIC profiles. From the relative energies listed in Table 2 it is immediately evident that a basically barrierless path conducts from the minimum over the TS to the S_1/S_0 CI seam. Having this information at hand, one wonders why then the relaxation of adenine is so sensitive to the excess energy imparted on the system.[8] By comparing the three TS geometries with the respective minima and the highest energy structures on the LIIC paths, one notices that in the TSs the $C6$ atom is less pyramidalized. In adenine, for example, the dihedral angle $\delta(C2N1C6C5)$ decreases from -19.0° for the highest LIIC to -9.7° for the TS structure. In other words, at the TS the distortion of the purine ring is localized on the carbon $C2$ atom. The relaxation from the geometry of vertical excitation to the S_1 minimum yields kinetic energy that needs to be redistributed among the vibrational modes (0.79 eV for adenine and $0.65 - 0.66$ eV for the monohydrates). Due to this excess kinetic energy, it is improbable that the relaxation will occur along the minimum energy path. In other words, the systems explore regions of their potential energy surfaces far from the LIIC or minimum energy pathways along which sizable barriers on the way to the S_1/S_0 CI seam exist. Thus, an efficient redistribution of vibrational energy to neighboring molecules should facilitate the internal conversion of adenine in solution.

Let us note that in order to minimize the basis set superposition error, optimizations

were also performed using the def2-QZVPP basis set. As can be seen from Table 2 (see also Figure S2), the energies of all minimum and transition state structures of the monohydrates remained almost unchanged (≤ 0.06 eV).

3.4 Electron driven relaxation pathways

From the above considerations it is apparent that the order of magnitude decrease of excited state lifetime in adenine monohydrates cannot be explained on the basis of efficient intermolecular redistribution of energy along the known ring-puckering pathways of adenine deactivation. Hence, we decided to investigate an alternative deactivation route for the dominant conformer $A(H_2O)^{N3}$. Specifically we focus on excited state PT (ESPT). It is known that ESPT plays a key role in the photochemistry of biomolecules[54] and its dynamics have been intensively investigated.[40,55–60] Ultrafast, barrierless PT reactions have been successfully simulated by surface hopping.[40,55,56] Moreover, the implemantation of the local diabatization formalism in surface hopping allows for efficient propagation of the wave function in regions of highly peaked nonadiabatic couplings.[60] However, as independent trajectories are used for the nuclear dynamics, tunneling through a barrier on the adiabatic potential surface cannot be described.

Figure 3 displays the reaction profile for proton transfer (PT) from water to the nitrogen atom $N3$. The leftmost point corresponds to the S_1 minimum energy geometry of $A(H_2O)^{N3}$. The TS for PT has been located 0.48 eV higher in energy. With respect to the FC geometry the TS is found 0.18 eV lower in energy. This makes the PT pathway classically allowed, but energetically less favorable than the ring-puckering pathways. With respect to accessibility, however, the PT pathway is strongly favored. The RMSD between the FC and TS geometries (3.7 Åamu$^{1/2}$) and between the FC and CI geometries of (3.5 Åamu$^{1/2}$) demonstrate that key PT geometries are easily accessible from the FC region. Moreover, most of the geometry deviation is due to water reorientation. If we consider only the displacement of the purine ring, the RMSD from the FC geometry are only 1.31 and 1.27 Åamu$^{1/2}$ for the TS and CI

geometries, respectively. We have estimated the water reorientation energy as the energy difference between two structures: the S_1 minimum and a structure in which water has been oriented as in the TS while the geometry of the S_1 minimum has been retained for the adenine ring. It turned out that water reorientation accounts for 0.4 eV out of 0.48 eV needed to surmount the barrier from the C_2 minimum to the TS. This clearly indicates that an accurate quantum mechanical treatment of the large amplitude inter-molecular motion is required. Such calculations are, however, beyond the scope of the present contribution.

A very interesting aspect of the PT pathway is the change of the character of the S_1 state along the reaction profile. From the insets in Figure 3 it is evident that the excitation is initially localized on the ring ($n\pi^*$) and that the charge transfer contribution increases along the reaction coordinate. At the TS geometry the transfer of negative charge from water to the purine ring is clearly visible signifying that the reaction at hand is an electron-driven proton transfer. Also we point out the stabilization of the S_2 state. In the region from TS to CI when the two fragments separate, the S_1 and S_2 states become degenerate as they correspond to excitation from the two oxygen lone pair orbitals to the purine ring π^* orbital. The ESPT pathway strongly resembles the water to chromophore electron transfer relaxation recently reported by Barbatti as the dominant relaxation mechanism of pentahydrated 7H-adenine. In that case, however, purely electronic transitions were reported as the lone pair orbitals were not aligned with the PT direction.

Altogether, after considering in detail the possible pathways of the deactivation of adenine monohydrates we found ESPT as a plausible relaxation mechanism, capable of explaining the observed ultrafast relaxation. Yet, none of the NA trajectories directly pointed to this pathway. This led us to question not only the reliability of the dynamics method, which is not based on the local diabatzation, but also the reliability of the electronic structure method. In this work we opted for the ADC(2) method owing to the known importance of $n\pi^*$ states in the relaxation of adenine and the need for an equilibrated treatment of all lone pair orbitals. The employment of ADC(2) turned out to be critical for the identification of the electron

driven PT mechanism. However, being a single reference method, ADC(2) cannot adequately describe bond fission. During NA dynamics this led to errors in the computation of energies and gradients, causing redistribution of energy within the water molecule and breaking of the free O-H bond. We have referred to this situation as water mediated relaxation and considered these trajectories unphysical due to the high D_1 values that they exhibit for a considerable span of time. The situation is somewhat different along the reaction path shown in Figure 3 where the D_1 diagnostic is slightly higher than the recommended value of $D_1 < 0.04$ (see Figure S1), but within the expected range for adenine. Note however that in $A(H_2O)^{N3}$, direct PT from water to adenine takes place. The TS structure has a biradical ground state and a barrier is encountered along the reaction path. This calls for a very accurate description of the adiabatic potential energy surface. Therefore, excitation energies of key ESPT geometries as well as those on the $C2$ and $C6$ ring-puckering pathways of adenine and $A(H_2)^{N3}$ were checked against CASPT2 calculations. The results are presented in Tables S8-S12. With respect to the $C2$ minimum, the barriers for proton transfer were evaluated as 0.65 and 0.73 eV, at the CAS-[14,10]/CASPT2 and CAS-[14,11]/CASPT2 levels, respectively. These are somewhat larger that the ADC(2) value of 0.48 eV. On the other hand, the TS for proton transfer was found to be 0.37 eV and 0.25 eV below the FC geometry, at the CAS-[14,10]/CASPT2 and CAS-[14,11]/CASPT2 levels, respectively, conforming the feasibility of ESPT. However we have assessed only a limited set of geometries that, due to excess kinetic energy, are probably not the ones that the system explores during the dynamics. Highly distorted geometries that are more likely to be encountered during the dynamics may not be adequately described with a single reference method such as ADC(2). From the contrasting results of NA dynamics simulations on adenine performed at different levels of theory (see Ref.[18]) it is clear that the outcome of the dynamics is very sensitive on the topography of the underlying potential energy surfaces. While ADC(2) is currently one of the best methods for dynamics simulations, multireference computations, from the one side, and conformer specific time resolved photoelectron imaging experiments, from the other,

may provide a new level of understanding and help disclosing the mechanism of ultrafast relaxation in adenine monohydrates.

4 Summary

We have explored possible mechanisms of excited-state deactivation of adenine monohydrates with the goal of identifying the ones responsible for the observed ultrafast decay. On the basis of nonadiabatic dynamics simulations and reaction path investigations we were able to show that the dominant deactivation mechanisms of adenine, $C2$ and $C6$ ring-puckerings, while active in the monohydrates, were not the ones responsible for the ultrafast, sub-100 fs, decay. Therefore we have focused on non-classical mechanisms and found that electron-driven proton transfer from water to adenine may be the mechanism leading to the sought ultrafast decay. Apart from the fact that the TS for PT is located below the geometry of vertical excitation, the accessibility of the electron driven PT pathway from the FC region, dynamical quantum effects, and the fragmentation of the adenine-water cluster observed in the experimental studies, are arguments in favor of this mechanism. Finally the ESPT pathway could be straightforwardly confirmed experimentally, as the absence of a deuteration effect on the experimental lifetimes would lead to its exclusion.

Testing the feasibility of the electron-driven proton transfer mechanism and providing a detailed characterization of the electronic states involved in the relaxation of adenine monohydrates opens prospects for future work and our understanding of the role of water in the excited state deactivation of nucleobases.

Acknowledgment

We are grateful to M. Barbatti and F. Plasser for providing us reference nonadiabatic dynamics results of gas phase adenine. The support from the Unity through Knowledge Fund (UKF B1) and the European COST Action CM1204 XLIC is acknowledged. Computer time

was provided by the Croatian National Grid Infrastructure (CRONGI) and the super- and high-performance computer facilities of the Suranaree University of Technology (SUT).

References

(1) Sobolewski, A. L.; Domcke, W. *Phys. Chem. Chem. Phys. - themed collection* **2010**, *12*, 4897.

(2) Markovitsi, D.; Sage, E.; Lewis, F. D.; Davies, J. *Photochem. Photobiol. Sci. - themed issue* **2013**, *12*, 1256.

(3) Kang, H.; Jung, B.; Kim, S. K. *J. Chem. Phys.* **2003**, *118*, 6717–6719.

(4) Ullrich, S.; Schultz, T.; Zgierski, M. Z.; Stolow, A. *J. Am. Chem. Soc.* **2004**, *126*, 2262–2263.

(5) Canuel, C.; Mons, M.; Piuzzi, F.; Tardivel, B.; Dimicoli, I.; Elhaninea, M. *J. Chem. Phys* **2005**, *122*, 074316/1–6.

(6) Bisgaard, C. Z.; Satzger, H.; Ullrich, S.; Stolow, A. *ChemPhysChem* **2009**, *10*, 101–110.

(7) Evans, N. L.; Ullrich, S. *J. Phys. Chem. A* **2010**, *114*, 11225–11230.

(8) Kang, H.; Chang, J.; Lee, S. H.; Ahn, T. K.; Kim, N. J.; Kim, S. K. *J. Chem. Phys.* **2010**, *133*, 154311/1–4.

(9) Kotur, M.; Weinacht, T. C.; Zhou, C.; Matsika, S. *IEEE J. Sel. Top. Quant. Electron.* **2012**, *18*, 187–194.

(10) Broo, A. *J. Phys. Chem. A* **1998**, *102*, 526–531.

(11) Sobolewski, A. L.; Domcke, W. *Eur. Phys. J. D* **2002**, *20*, 369–374.

(12) Perun, S.; Sobolewski, A. L.; Domcke, W. *J. Am. Chem. Soc.* **2005**, *127*, 6257–6265.

(13) Serrano-Andrés, L.; Merchán, M.; Borin, A. C. *Proc. Natl. Acad. Sci. U.S.A.* **2006**, *103*, 8691–8696.

(14) Chung, W. C.; Lan, Z. G.; Ohtsuki, Y.; Shimakura, N.; Domcke, W.; Fujimura, Y. *Phys. Chem. Chem. Phys.* **2007**, *9*, 2075–2084.

(15) Fabiano, E.; Thiel, W. *J. Phys. Chem. A* **2008**, *112*, 6859–6863.

(16) Barbatti, M.; Lischka, H. *J. Am. Chem. Soc.* **2008**, *130*, 6831–6839.

(17) Conti, I.; Garavelli, M.; Orlandi, G. *J. Am. Chem. Soc.* **2009**, *131*, 16108–16118.

(18) Barbatti, M.; Lan, Z.; Crespo-Otero, R.; Szymczak, J. J.; Lischka, H.; Thiel, W. *J. Chem. Phys.* **2012**, *137*, 22A503/1–14.

(19) Picconi, D.; Avila-Ferrer, F. J.; Improta, R.; Lami, A.; Santoro, F. *Faraday Discuss.* **2013**, *163*, 223–242.

(20) Plasser, F.; Crespo-Otero, R.; Pederzoli, M.; Lischka, J. P. H.; Barbatti, M. *J. Chem. Theory Compt.* **2014**, *10*, 1395–1405.

(21) Schirmer, J. *Phys. Rev. A* **1982**, *26*, 2395–2416.

(22) Trofimov, A. B.; Schirmer, J. *Chem. Phys.* **1997**, *214*, 153–170.

(23) Cohen, B.; Hare, P. M.; Kohler, B. *J. Am. Chem. Soc.* **2003**, *125*, 13594–13601.

(24) Mitrić, R.; Werner, U.; Wohlgemuth, M.; Seifert, G.; Bonačić-Koutecký, V. *J. Phys. Chem. A* **2009**, *113*, 12700–12705.

(25) Ludwig, V.; da Costa, Z. M.; do Amaral, M. S.; Borin, A. C.; Canuto, S.; Serrano-Andres, L. *Chem. Phys. Lett.* **2010**, *492*, 164–169.

(26) Conti, I.; Altoé, P.; Stenta, M.; Garavelli, M.; Orlandi, G. *Phys. Chem. Chem. Phys.* **2010**, *12*, 5016–5023.

(27) Lan, Z.; Lu, Y.; Fabiano, E.; Thiel, W. *ChemPhysChem* **2011**, *12*, 1989–1998.

(28) Barbatti, M. *J. Am. Chem. Soc.* **2014**, *136*, 10246–10249.

(29) Kang, H.; Lee, K. T.; Kim, S. K. *Chem. Phys. Lett.* **2002**, *359*, 213–219.

(30) Ritze, H.-H.; Lippert, H.; Samoylova, E.; Smith, V. R.; Hertel, I. V.; Radloff, W.; Schultz, T. *J. Chem. Phys.* **2005**, *122*, 224320/1–9.

(31) Nosenko,; Kunitski, M.; Riehn, C.; Harbach, P. H. P.; Dreuw, A.; Brutschy, B. *Phys. Chem. Chem. Phys.* **2010**, *12*, 863–870.

(32) Hättig, C.; Weigend, F. *J. Chem. Phys.* **2000**, *113*, 5154–5161.

(33) Hättig, C.; Hellweg, A.; Köhn, A. *Phys. Chem. Chem. Phys.* **2006**, *8*, 1159–1169.

(34) Dunning, T. H. *J. Chem. Phys.* **1989**, *90*, 1007–1023.

(35) Tully, J. C. *J. Chem. Phys.* **1990**, *93*, 1061–1071.

(36) Curchod, B. F. E.; Rothlisberger, U.; Tavernelli, I. *ChemPhysChem* **2013**, *14*, 1314–1340.

(37) Novak, J.; Mališ, M.; Prlj, A.; Ljubić, I.; Kühn, O.; Došlić, N. *J. Phys. Chem. A* **2012**, *116*, 11467–11475.

(38) Sapunar, M.; Ponzi, A.; Chaiwongwattana, S.; Mališ, M.; Prlj, A.; Decleva, P.; Došlić, N. *Phys. Chem. Chem. Phys.* **2015**, *17*, 19012–19020.

(39) *TURBOMOLE V7.0 2015, a development of University of Karlsruhe and Forschungszentrum Karlsruhe GmbH, 1989-2007, TURBOMOLE GmbH, since 2007, available from http://www.turbomole.com.*

(40) Tuna, D.; Došlić, N.; Mališ, M.; Sobolewski, A. L.; Domcke, W. *J. Phys. Chem. B* **2015**, *119*, 21122124.

(41) Shampine, L.; Gordon, M. *Computer Solution of Ordinary Differential Equations: The Initial Value Problem*; Freeman, 1975.

(42) Granucci, G.; Persico, M. *J. Chem. Phys.* **2007**, *126*, 134114/1–11.

(43) Tannor, J., David *Introduction to quantum mechanics: a time-dependent perspective*; University Science Books: Sausalito, CA, 2007.

(44) Došlić, N.; Bosanac, S. *Mol. Phys.* **1997**, *90*, 599–609.

(45) Sun, L.; Hase, W. L. *J. Chem. Phys.* **2010**, *133*, 044313.

(46) Janssen, C. L.; Nielsen, I. M. *Chem. Phys. Lett.* **1998**, *290*, 423–430.

(47) Levine, B. G.; Coe, J. D.; Martínez, T. J. *J. Phys. Chem. B* **2008**, *112*, 405–413.

(48) Helgaker, T. *Chem. Phys. Lett.* **1991**, *182*, 503–510.

(49) Weigend, F.; Furche, F.; Ahlrichs, R. *The Journal of Chemical Physics* **2003**, *119*, 12753–12762.

(50) Werner, H.; Knowles, P. J.; Knizia, G.; Manby, F. R.; Schütz, M. *Wiley Interdisciplinary Reviews: Computational Molecular Science* **2012**, *2*, 242–253.

(51) Hanus, M.; Kabeláč, M.; Rejnek, J.; Ryjáček, F.; Hobza, P. *J. Phys. Chem. B* **2004**, *108*, 2087–2097.

(52) Clark, L. B.; Peschel, G. G.; Tinoco, I. *J. Phys. Chem.* **1965**, *69*, 3615–3618.

(53) Crespo-Hernández, C. E.; Martínez-Fernández, L.; Rauer, C.; Reichardt, C.; Mai, S.; Pollum, M.; Marquetand, P.; González, L.; Corral, I. *J. Am. Chem. Soc.* **2015**, *137*, 4368–4381.

(54) Sobolewski, A. L.; Domcke, W. *J. Phys. Chem. A* **2007**, *111*, 11725–11735.

(55) Guglielmi, M.; Tavernelli, I.; Rothlisberger, U. *Phys. Chem. Chem. Phys.* **2009**, *11*, 4549–4555.

(56) Daengngern, R.; Kungwan, N.; Wolschann, P.; Aquino, A. J. A.; Lischka, H.; Barbatti, M. *J. Phys. Chem. A* **2011**, *115*, 14129–14136.

(57) Kungwan, N.; Plasser, F.; Aquino, A. J. A.; Barbatti, M.; Wolschann, P.; Lischka, H. *Phys. Chem. Chem. Phys.* **2012**, *14*, 9016–9025.

(58) Basarić, N.; Došlić, N.; Ivković, J.; Wang, Y.; Mališ, M.; Wan, P. *Chem. Eur. J.* **2012**, *18*, 10617–10623.

(59) Basarić, N.; Došlić, N.; Ivković, J.; Wang, Y.; Veljković, J.; Mlinarić-Majerski, K.; Wan, P. *J. Org. Chem.* **2013**, *78*, 1811–1823.

(60) Plasser, F.; Granucci, G.; Pittner, J.; Barbatti, M.; Persico, M.; Lischka, H. *J. Chem. Phys.* **2012**, *137*, 22A514–13.

Table 1: ADC(2)/aug-cc-pVDZ vertical excitation energies and oscillator strengths for adenine (A) and adenine-monohydrates ($A(H_2O)^{N3}$ and $A(H_2O)^{N7}$). Adiabatic excitation energies to the S_1 minimum are given in parenthesis.

	A		$A(H_2O)^{N3}$		$A(H_2O)^{N7}$	
State	E/eV	f	E/eV	f	E/eV	f
$n\pi^*$	4.98 (4.30)	0.013	5.11	0.002	5.02	0.001
$\pi\pi^*(L_a)$	5.09	0.250	5.04 (4.38)	0.279	4.90 (4.25)	0.245
$\pi\pi^*(L_b)$	5.11	0.036	5.11	0.029	5.08	0.055
πRyd	5.39	0.010	5.48	0.012]	5.27	0.005

Table 2: Relative energies of the relevant geometries along the $C2$, $C6$ and proton transfer relaxation pathways given with respect to the energy of vertical excitation to the bright $\pi\pi^*$ state. The energies are given for the S_1 minima ($E_{FC}^{S1_{min}}$), conical intersections (E_{FC}^{CI}), the barriers on the LIIC to the CI (E_{FC}^{B}) and the corresponding optimised transition states (E_{FC}^{TS}). Computations were performed at the ADC(2)/aug-cc-pVDZ and ADC(2)/def2-QZVPP (reported within parentheses) levels.

System	$E_{FC}^{S1_{min}}$	CI	E_{FC}^{CI}	E_{FC}^{B}	E_{FC}^{TS}
A	-0.79 (-0.67)	$C2$	-0.97	-0.25	-0.62 (-0.55)
		$C6$	-0.96	-0.02	-0.60 (-0.54)
$A(H_2O)^{N3}$	-0.66 (-0.67)	$C2$	-1.09	-0.32	-0.62 (-0.56)
		$C6$	-1.10	0.10	-0.59 (-0.60)
		PT	-1.35		-0.18 (-0.14)
$A(H_2O)^{N7}$	-0.62 (-0.68)	$C2$	-0.95	-0.27	-0.53 (-0.54)
		$C6$	-0.90	0.19	-0.54 (-0.59)

Table 3: Fraction of trajectories returning to the ground state by the main deactivation mechanisms. Other refers to H-elimination in A (averaged over two domains) and to water mediated relaxation in $A(H_2O)^{N3}$ and $A(H_2O)^{N7}$

	A^a	$A(H_2O)^{N3}$	$A(H_2O)^{N7}$
$C2$	0.53	0.42	0.54
$C6$	0.39	0.21	0.23
other	0.08	0.38	0.23

[a]Reference [20]

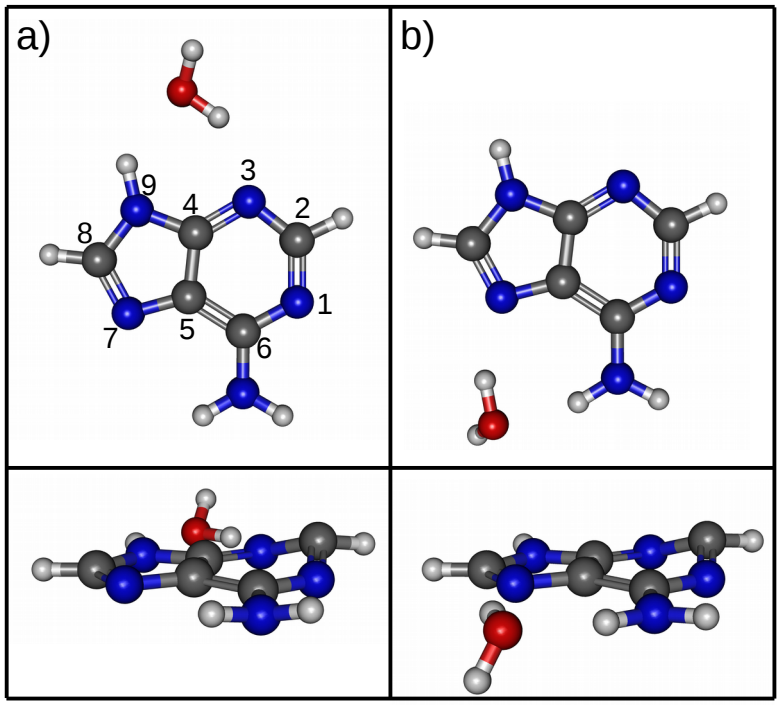

Figure 1: Geometries of adenine monohydrates $A(H_2O)^{N3}$ (a) and $A(H_2O)^{N7}$ (b) optimized in the ground state (upper) and the first excited state (lower) at the MP2(ADC(2))/aug-cc-pVDZ level.

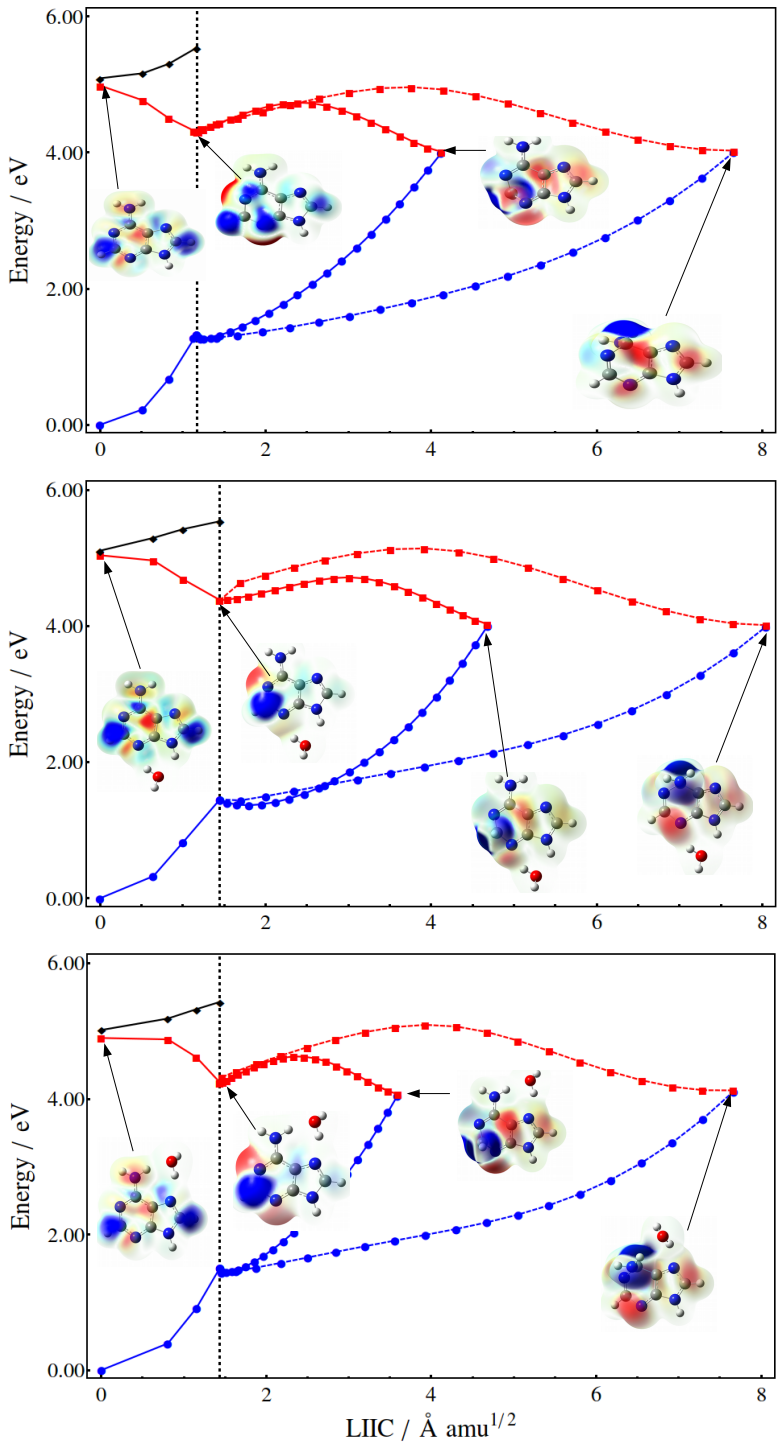

Figure 2: Linear interpolation in internal coordinates (LIIC) reaction paths for adenine (upper), $A(H_2O)^{N3}$ (middle) and $A(H_2O)^{N7}$ (lower). Interpolation was performed between the FC geometry and the S_1 minimum (left of the dashed black line), and between the minimum and $C2/C6$ CIs (right). Density differences between the excited and the ground state are given at key points along the paths.

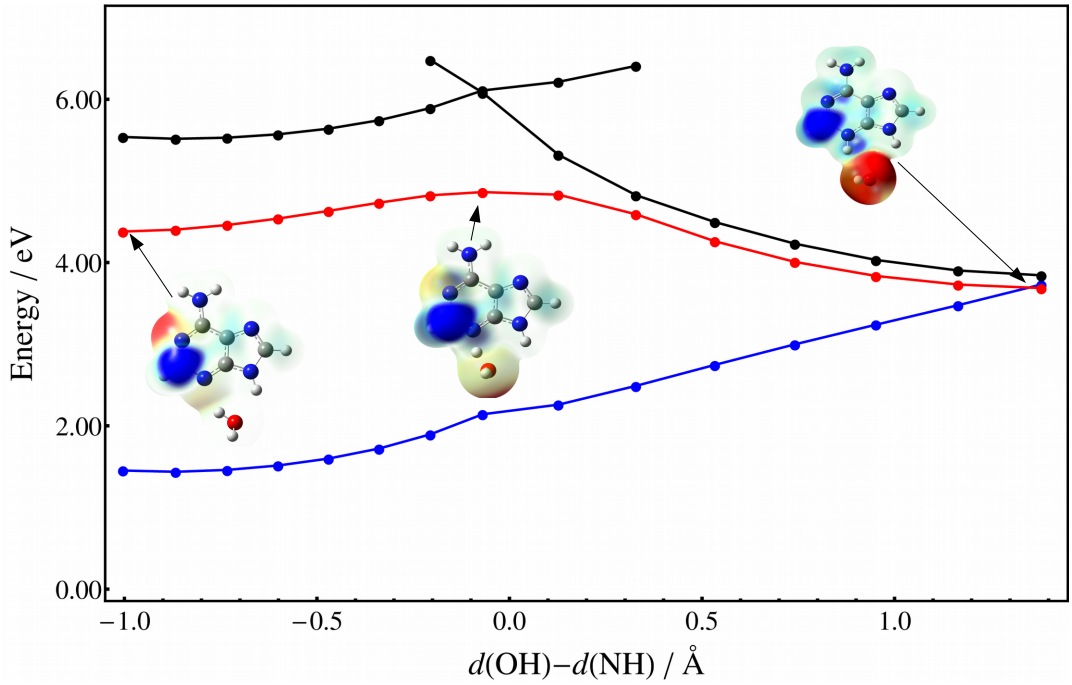

Figure 3: LIIC showing the electron driven proton transfer pathway in $A(H_2O)^{N3}$. Interpolation was performed from the S_1 minimum to the TS, and from the TS to the CI. S_0 (blue), $n\pi^*$ (red), $\pi\pi^*$ (black) and charge transfer (CT) state (black). The $\pi\pi^*/CT$ CI is found at the TS geometry (crossing of two black lines). Electron density difference plots showing the change of character of the excited state are given in the insets.